Electrochimica Acta 229 (2017) 352–360

Contents lists available at ScienceDirect

Electrochimica Acta

journal homepage: www.elsevier.com/locate/electacta

Hierarchical Porous Carbon Materials Derived from Self-Template Bamboo Leaves for Lithium–Sulfur Batteries

Yuanyuan Li[a], Lei Wang[a], Biao Gao[b], Xingxing Li[b], Qifa Cai[a], Qingwei Li[a,c], Xiang Peng[c], Kaifu Huo[a,*], Paul K. Chu[c,*]

[a] Wuhan National Laboratory for Optoelectronics, School of Optical and Electronic Information, Huazhong University of Science and Technology, Wuhan 430074, People's Republic of China
[b] The State Key Lab for Refractory and Metallurgy, Wuhan University of Science and Technology, Wuhan 430081, People's Republic of China
[c] Department of Physics and Materials Science, City University of Hong Kong, Tat Chee Avenue, Kowloon, Hong Kong, China

ARTICLE INFO

Article history:
Received 19 October 2016
Received in revised form 18 January 2017
Accepted 25 January 2017
Available online 26 January 2017

Keywords:
Self-template
bamboo leaves
hierarchical porous carbon
mesoporous SiO_2 nanoparticles
lithium-sulfur batteries

ABSTRACT

Lithium-sulfur (Li-S) batteries are attractive and promising energy storage devices due to the large theoretical energy density (2600 Wh kg^{-1}) and natural abundance of sulfur. However, several intrinsic drawbacks hamper broader application, for example, the poor conductivity, serious shuttle effect, as well as large volume expansion. In this work, hierarchical porous carbon materials (HPCMs) are prepared from natural bamboo leaves by carbonization and HF etching. The biogenetic SiO_2 nanoparticles (NPs) with abundant mesopores in the carbonized bamboo leaves are etched by HF producing hierarchical meso-/microporous carbon that can be exploited to load sulfur on the nanoscale. The HPCMs/S composite loaded with 70.26 wt. % sulfur shows a high initial discharge capacity of 1487 mAh g^{-1} at a rate of 0.05C (1C = 1675 mA g^{-1}) and the capacity of 707 mAh g^{-1} is maintained at 1C for over 200 cycles with a capacity decay of only 0.014% per cycle. When the current density is increased from 0.2 to 4C, 62.3% of the capacity is retained, suggesting good rate capability and promising application to advanced Li-S batteries.

1. Introduction

The rapidly expanding market of portable electronics, electrical vehicles (EVs), and large-scale smart grids has stimulated the advance of energy storage technology and devices [1]. Lithium-sulfur (Li-S) batteries are promising energy storage devices due to the large theoretical energy densities (2600 Wh kg^{-1}) that are 3-5 times bigger than those of state-of-art lithium-ion batteries composed of graphite anodes and $LiCoO_2$/$LiFePO_4$ cathodes [2]. Moreover, S is abundant, cheap, and nontoxic, the production cost of Li-S batteries is relatively low [3]. However, S cathodes have some inherent drawbacks including the poor electron conductivity of elemental S and its discharged products, serious shuttle effect of the polysulfide intermediates, and large volume expansion of S during cycling. The low conductivity of S and its discharged products results in low utilization of S and poor rate capability [4]. Moreover, the polysulfide intermediates are soluble in the electrolyte and shuttle back and forth between the cathode and anode during charging and discharging causes loss of active S, poor capacity retention, low coulombic efficiency, as well as corrosion of the lithium anode [5]. A remedy is to combine S with conductive host materials such as carbonaceous materials to enhance the Li storage properties of S-based cathodes by improving the conductivity of the electrode and mitigating the polysulfides shuttle effect [6–19]. Among the various types of carbonaceous materials, hierarchical porous carbon are particularly attractive as the S host or matrix materials because the high conductivity of hierarchical carbon enhances the conductivity of the cathode and the porous structure improves the S mass loading and inhibits the shuttle effect of polysulfide intermediates. Various sulfur/hierarchically porous carbon (S/HPCs) have been fabricated for Li−S cathodes. For instance, Rehman et al. prepared vertically aligned and interconnected porous carbon nanosheets with macrovoids, mesopores, and micropores by carbonization of agar and KOH [20] and Li et al. reported a facile *in situ* method to synthesize three-dimensional (3D) porous graphitic carbon composites containing sulfur nanoparticles using glucose, NaCl and Na_2S crystals [21]. However, the typical synthesis process of porous carbon materials, such as mesoporous CMK-3 [22,23] tends to be complex and costly and lacks scalability and consistency.

* Corresponding authors.
E-mail addresses: kfhuo@hust.edu.cn (K. Huo), paul.chu@cityu.edu.hk (P.K. Chu).

http://dx.doi.org/10.1016/j.electacta.2017.01.166
0013-4686/

Biomass, as an important resource of porous carbon materials, has attracted increasing attention on account of the abundance, sustainability, and low cost [24]. Hydrothermal carbonization is the most popular route to convert biomass to porous carbon. For example, porous carbon spheres were synthesized through hydrothermal carbonization and KOH chemical activation using glucose as the precursors by Guo's group [25] and Feng et al. prepared hierarchical carbon derived from bagasse waste by silica-assisted hydrothermal carbonization in combination with KOH activation [26]. However, these approaches typically require a long time, high pressure, and high temperature. Furthermore, carbon materials produced by hydrothermal carbonization generally need further KOH chemical activation [27–29] or the use of silica [30] as templates to create the pores thereby raising the process complexity and cost. Bamboo, one of the abundant natural resources due to fast growth and short maturity cycle [31], is a natural reservoir of nanostructured SiO_2 by absorbing water-soluble silicic acid and then converting into hydrate SiO_2 nanoparticles (NPs) that are mainly accumulated in the leaves by biomineralization [32]. The biogenetic SiO_2 NPs in the bamboo leaves have abundant mesopores and the content of SiO_2 is 13–41 wt.% depending on the species, climate, and geographical location [32,33]. In general, the connected 3D microstructure in the bamboo leaves consisting of hydrate SiO_2 NPs, cellulose, semicellulose, and lignin provide a good template for the formation of hierarchical porous carbonaceous structures *via* carbonization and subsequent removal of the mesoporous SiO_2 NPs.

Herein, we describe a self-template strategy to produce hierarchical porous carbon materials (HPCMs) derived from bamboo leaves by carbonization and etching in HF, which are further used as a host material to load S as high-performance cathode material for Li-S batteries. The bamboo leaves derived HPCMs have a large surface area, high conductivity, 3D connectivity and order at the nanoscale boding well for Li-S batteries. The mesovoids derived from the mesoporous SiO_2 NPs could encapsulate nanoscale S and the S mass loading is about 70.26 wt.%. The HPCMs/S composite shows a large discharge capacity of 775 mAh g^{-1} at a rate of 0.5C (1C = 1675 mA g^{-1}) for over 100 cycles, which is better than that of the sublimed S cathode (only 414 mAh g^{-1} after 100 cycles). Moreover, the HPCMs/S composite maintains a discharge capacity of 707 mAh g^{-1} at a rate of 1C for over 200 cycles. The capacity decay is only 0.014% per cycle and 62.3% of the capacity is retained when the current density is increased from 0.2 to 4C thus revealing high rate capability and good cycle stability.

2. Experimental Section

2.1. Materials Preparation

2.1.1. Synthesis of hierarchically porous carbon materials (HPCMs)

The bamboo leaves were collected from bamboo gardens in Wuhan University of Science and Technology (Wuhan, China). In the typical synthesis, the bamboo leaves were cleaned with distilled water and dried at 100 °C in the oven for 24 h. They were then boiled at 100 °C in 1 M HCl for 2 h to remove metal impurities. The acid-etched bamboo leaves were rinsed with distilled water until the pH was neutral, which are further annealed at 800 °C for 2 h in a tube furnace under Ar. Finally, the carbonized bamboo leaves were soaked in 5% HF to remove the biogenetic SiO_2 templates, rinsed with deionized water, and dried in an oven at 100 °C to produce HPCMs.

2.1.2. Preparation of HPCMs/S composites

The HPCMs/S composites were prepared by a conventional melting diffusion strategy. Briefly, the as-prepared HPCMs and sublimed S powders were mixed (weight ratio of 1:2.5), ground in an agate mortar, and sealed in a vacuum glass tube. The tube was heated at 155 °C for 12 h in a muffle furnace to produce HPCMs/S composites.

2.2. Materials Characterization

The morphology, structure, and composition of the samples were characterized by field-emission scanning electron microscopy (FE-SEM, Nano SEM 450), transmission electron microscopy (TEM, Tecnai G20), energy-dispersive X-ray spectroscopy (EDS, Oxford INCA 200), X-ray diffraction (XRD, Philips X'Pert Pro), Raman scattering (HR RamLab) and X-ray photoelectron spectroscopy (XPS, AXIS-ULTRA DLD-600W). The nitrogen adsorption-desorption isotherms and pore size distribution were obtained by the Brunauer-Emmett-Teller nethod (BET, Micrometrics, ASAP2010) at 77 K and the S content in the HPCMs/S composite was determined by thermogravimetric analysis (TGA, NETZSCH, TG 209 F3).

2.3. Electrochemical tests

To prepare the working electrodes, the HPCMs/S composite was mixed with acetylene black and polyvinylidene fluoride (PVDF) at a weight ratio of 80:10:10 and then *N*-2-methylpyrrolidinone (NMP) was added dropwise to form a slurry. The homogeneous slurry was casted onto aluminum current collectors (15 μm thickness) by the blade doctor method, followed by vacuum drying at 60 °C for 12 h and punching into round cathodes. The average sulfur loading on each electrode was around 1.8 mg cm^{-2}. The HPCMs/S composite had a sulfur content of 70.26 wt.% and the prepared whole cathode has a sulfur content of 56.21 wt.%. For comparison, the pure S cathode was prepared by a similar procedure by mixing 50 wt.% sublimed sulfur, 40 wt.% acetylene black, and 10 wt.% PVDF. The CR2016-type coin cells were assembled in an argon-filled glove box under water and oxygen below 0.1 ppm. The lithium metal was the counter electrode and the polypropylene membrane (Celgard 2400) served as the separator. The electrolyte was 1 M bis (trifluoromethane)sulfonylimide lithium (LiTFSI) with 1 wt.% $LiNO_3$ as the additive dissolved in the mixture of dimethoxyethane (DME) and 1,3-dioxolane (DOL) (1:1 by volume) (Beijing Institute of Chemistry, Beijing, China). Cyclic voltammetry (CV) was performed on an electrochemical workstation (CHI 660E, Shanghai, China) at a scanning rate of 0.1 mV s^{-1} between 1.7 and 2.8 V versus Li^+/Li and electrochemical impedance spectroscopy (EIS) was conducted on the same instrument at frequencies between 100 kHz and 0.01 Hz with an amplitude of 5 mV. The galvanostatic charging-discharging (GCD) tests were carried out on the Xinwei instrument (Shenzhen, China) and the cutoff voltage was controlled from 1.7 to 2.8 V versus Li^+/Li. The specific capacity values were calculated on the basis of the mass of the active sulfur (1 C = 1675 mA g^{-1}) and all of the electrochemical tests were performed at room temperature.

3. Results and Discussion

The synthetic procedures of the HPCMs and HPCMs/S composites are illustrated in Scheme 1. The as-collected bamboo leaves are firstly boiled in HCl to remove metallic impurities. The thermogravimetric analysis results of the HCl-etched bamboo leaves under Ar/O_2 atmosphere are shown in Fig. S1. The weight loss from room temperature to 200 °C is 2.17 wt.% stemming from evaporation of water and those of 45.13 wt.% and 32.27 wt.% from 200 to 600 °C arise from decomposition and oxidation of small and large organic molecules, respectively [34]. The content of SiO_2 in the HCl-etched bamboo leaves is about 20.43 wt.%. The HCl-etched bamboo leaves were further annealed under Ar in a tube furnace

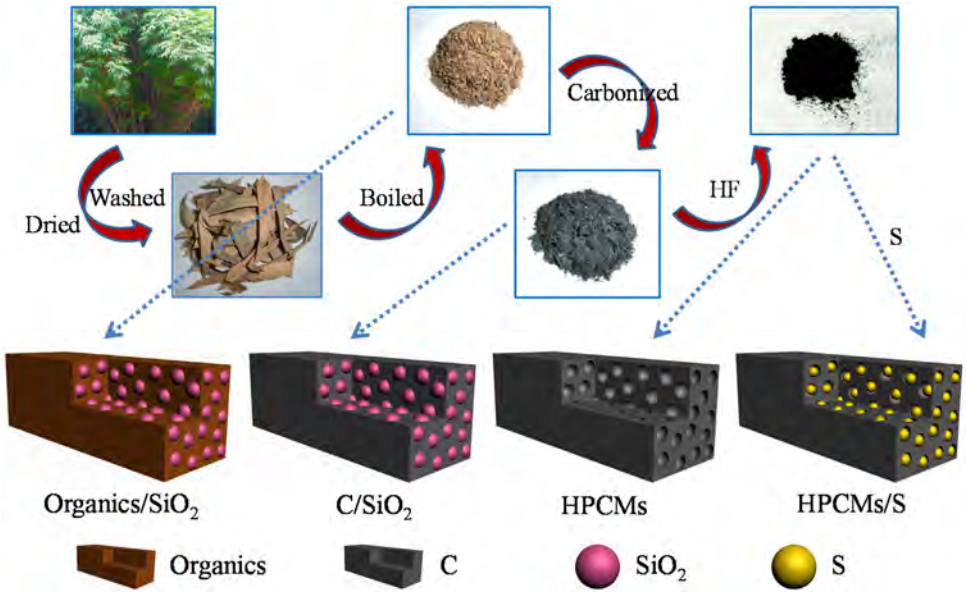

Scheme 1. Schematic illustration of the preparation of hierarchically porous carbon materials (HPCMs) and HPCMs/S composites from bamboo leaves.

and subsequently immersed in HF to etch the mesoporous SiO_2 templates to produce hierarchical meso-/microporous carbon materials. The HPCMs/S is prepared by melt diffusion and most of S particles occupy the nanovoids mainly derived from the templates of mesoporous SiO_2 in the bamboo leaves. This technique utilizes the natural 3D self-template of the bamboo leaves to produce HPCMs without additional activation, which provide an economic, controllable and sustainable route for the production of HPCMs/S for Li-S batteries.

Fig. S2a and b depict the FE-SEM images of carbonized bamboo leaves revealing plate-like morphology with coarse surface and many protrusions. The EDS map in Fig. S2c discloses that C, O, and Si are also uniformly distributed in the bamboo leaves. The TEM image (Fig. S2d) of the carbonized bamboo leaves indicates SiO_2 nanoparticles (NPs) with diameters of 10–30 nm are uniformly distributed into carbon matrix. HPCMs are produced via etching the mesoporous SiO_2 of carbonized bamboo leaves in HF solution. Fig. 1a reveals that the HPCMs have a plate-like morphology with a size of several micrometers and the enlarged FE-SEM image discloses that there are numerous crosslinked small pores generated after etching mesoporous SiO_2 (Fig. 1b). TEM images in Fig. 1c and d further confirm the formation of hierarchically

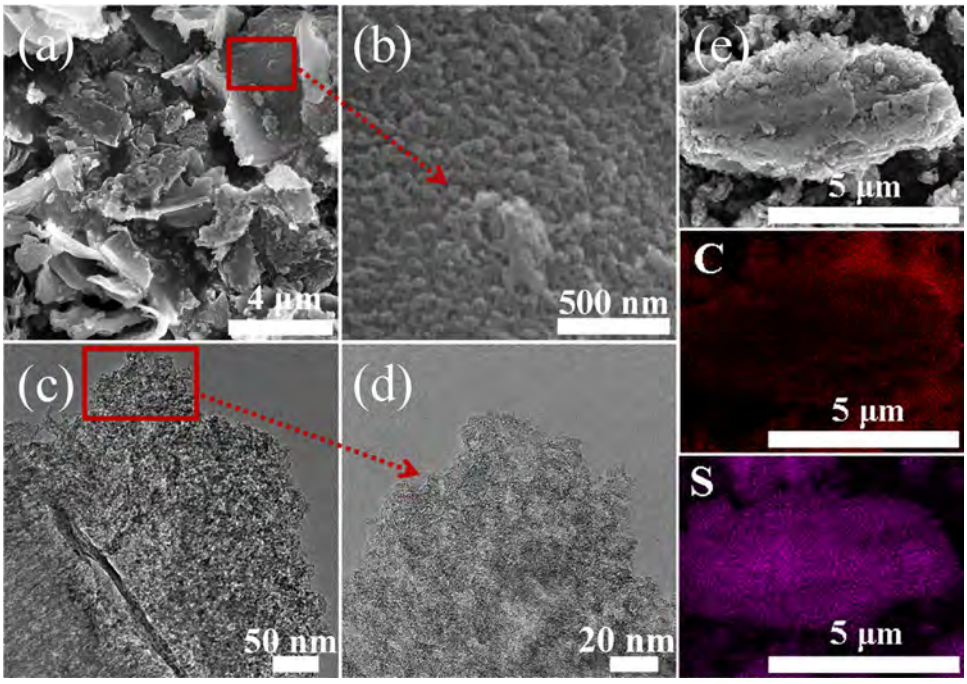

Fig. 1. (a and b) Low and high-magnification FE-SEM images of HPCMs; (c and d) Low and high-magnification TEM images of HPCMs; (e) EDS map of the HPCMs/S.

porous structure. The HPCMs derived from the bamboo leaves are good host materials to load S for Li-S batteries and Fig. 1e indicates that S is dispersed uniformly in the HPCMs.

The nitrogen adsorption-desorption isotherms and corresponding pore size distributions of the HPCMs and HPCMs/S are displayed in Fig. 2. The adsorption-desorption isotherm of HPCMs reveals microporous and mesoporous characteristics and the pore distribution is 0.5–30 nm (Fig. 2a and b). The HPCMs have a BET surface area of 284 $m^2 g^{-1}$ and pore volume of 0.6 $cm^3 g^{-1}$ (0.08 $cm^3 g^{-1}$ for micropores and 0.52 $cm^3 g^{-1}$ for mesopores). However, the carbonized HCl-etched bamboo leaves (before the removal of the SiO_2) only has a surface area of 32 $m^2 g^{-1}$ (Fig. S3a). We also measured the BET surface area and pore volume of the biogenetic SiO_2 after the removal of carbon at 700 °C for 2 h in air and the BET surface area and pore volume of SiO_2 NPs derived from bamboo leaves are 329 $m^2 g^{-1}$ and 0.5 $cm^3 g^{-1}$, respectively, corroborating that the SiO_2 NPs are abundant mesopores (Fig. S3b and c). During the biomineralization for the formation of SiO_2 nanoparticles, the organic moleculars in the bamboo leaves are interpenetrated into the mesopores of hydrate SiO_2 NPs producing inter-connected organic network. After carbonization under Ar and removal of mesoporous SiO_2 nanoparticles, the carbonized carbon materials within the mesoporous SiO_2 are exposed, producing the interconnected meso-/microporous carbon. This is the main reason why we could not observe the remaining cavity with the similar size of SiO_2 NPs in the TEM image of HPCMs (Fig. 1c and d). Moreover, the HPCMs and the mesoporous SiO_2 derived from bamboo leaves have the similar pore-size distribution (Figs. 2 and S3c). Therefore, it is safe to conclude that the mesoporosity of the HPCMs results from the removal of mesoporous SiO_2 and the microporousity of the HPCMs stems from the carbonization of the organic biomass due to the shrinking of organic materials and the removal of the hydrogen and the small organic molecules during carbonization [35]. After S incorporation, the surface area and pore volume of the HPCMs/S composite diminish to 63 $m^2 g^{-1}$ and 0.08 $m^3 g^{-1}$, respectively, indicating that S is embedded in or encapsulated into the

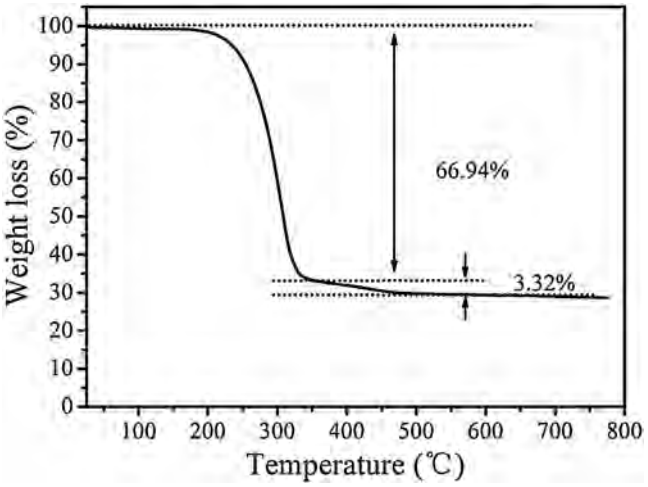

Fig. 3. Thermogravimetric analysis (TGA) curves of HPCMs/S composites from room temperature to 800 °C at a heating rate of 5 °C/min under Ar.

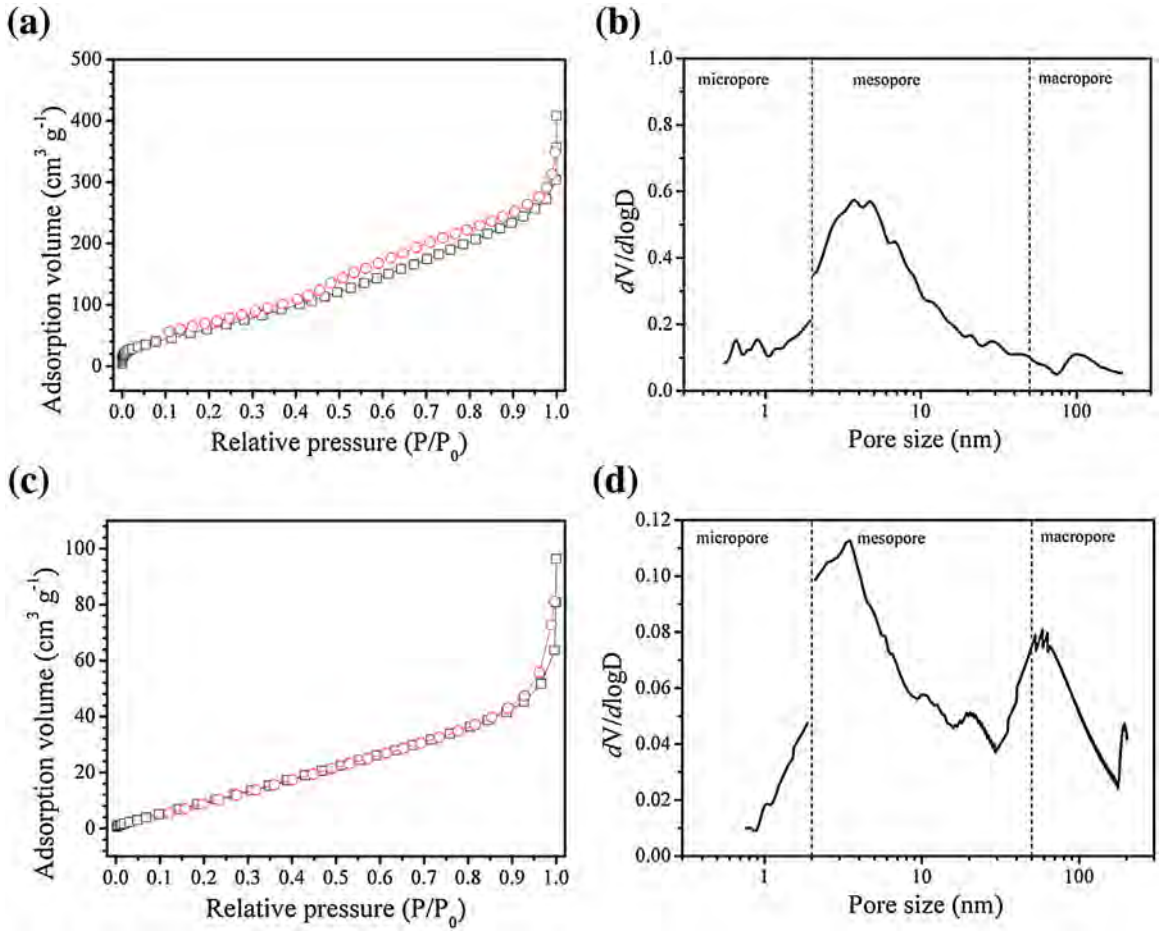

Fig. 2. Nitrogen adsorption-desorption isothermal curves of (a) HPCMs and (c) HPCMs/S; Corresponding pore size distribution plots of (b) HPCMs and (d) HPCMs/S.

micropores and mesopores (Fig. 2c and d). The increase of relative content of macropores in Fig. 2d after sulfur loading is due to the unavoidable presence of surface S onto HPCMs during melting infiltration. The thermogravimetirc curve in Fig. 3 shows that the HPCMs/S composite has a high S mass loading of 70.26 wt.%. The large weight loss of 66.94 wt. % from 200 to 350 °C is attributed to S infiltration into the mesopores or surface S and the small weight loss of 3.32 wt% from 350 to 500 °C arises from S being embedded into the micropores.

Fig. 4 displays the XRD patterns and Raman scattering spectra of the sublimed S, HPCMs, and HPCMs/S composites. The sublimed S shows strong S diffraction peaks (Fig. 4a) (JCPDS Card No. 08-0247). The broad peak between 20° and 30° observed from HPCMs is ascribed to the (002) peak of amorphous carbon. After S infiltrated, the HPCMs/S shows sharp and strong sulfur signals and reduced intensity of the HPCMs diffraction peaks, implying that S is incorporated into the HPCMs. Raman spectra depicted in Fig. 4b exhibits three peaks of sublimed S at 150, 215 and 470 cm^{-1} and two characteristic peaks of HPCMs (D and G bands at 1360 cm^{-1} and 1590 cm^{-1}, respectively). After S incorporation, both the C and S signals in the HPCMs/S composites decrease slightly, further corroborating that S is embedded into the HPCMs.

The electrochemical properties of the HPCMs/S and S cathodes are evaluated using CR2016-type coin cells. Fig. 5a shows the CV profiles of the HPCMs/S cathode in the voltage window between 1.7 and 2.8 V versus Li^+/Li at a scanning rate of 0.1 mV s^{-1}. There are two pairs of oxidation and reduction peaks. In the first cycles, reduction peaks at 2.26 and 2.00 V and oxidation peaks at 2.35 and 2.42 V are observed. From the 2nd to 10th cycles, the redox peak positions are nearly unchanged implying good reversibility. The two cathodic peaks at 2.31 and 2.01 V are attributed to the formation of long-chain soluble lithium polysulfide (Li_2S_n, $4 \leq n \leq 8$) and short-chain insoluble lithium sulfide (Li_2S_2 or Li_2S), respectively. The anodic peaks at 2.33 and 2.39 V suggest two oxidation processes from Li_2S to long-chain lithium polysulfide (Li_2S_n) and S. The integrated CV areas calculated from the HPCMs/S cathode increase gradually from the 1st to 10th cycles, suggesting gradual electrochemical activation of the HPCMs/S cathode upon cycling. The CV curves of the sublimed S cathode are depicted in Fig. 5b. In the initial cycle, the cathodic and anodic peaks are at 2.17, 1.91 V and 2.40, 2.44 V, respectively, and after 10 cycles, the reduction peaks and oxidation peaks are at 2.28, 1.99 V and 2.41, 2.45 V, respectively, implying larger polarization due to the poor conductivity. Fig. 5c and d display the GCD profiles of the HPCMs/S and sublimed S cathodes. The first three cycles are activated at 0.05C (1C = 1675 mA g^{-1}) and the others are measured at a rate of 0.5C. The 1st and 2nd lithiation capacities of the HPCMs/S cathode at a rate of 0.05C are 1487 and 1332 mAh g^{-1} with the coulombic efficiency (CE, delithiation capacities/lithiation capacities) of 85.0% and 90.7%, respectively (Fig. 5c). When the discharge voltage is less than 1.90 V at a low activated rate of 0.05C, there are long tails which disappear as the current density is raised to 0.5C due to decomposition of $LiNO_3$ additives [36,37] and the strong adsorption process of Li_2S_2/Li_2S in the micropores [20,23,38–40]. The lithiation capacity at the 5th cycle is 776 mAh g^{-1} and maintains at 775 mAh g^{-1} for over 100 cycles with a capacity retention rate of 99.9%. Different from HPCMs/S, the sublimed S cathode exhibits high initial and second discharge specific capacities of 1639 and 1482 mAh g^{-1} at a rate of 0.05C with the CE of 84.0% and 79.6%, respectively (Fig. 5d). However, the capacity rapidly drops to 414 mAh g^{-1} after 100 cycles with only 51.8% of the capacity retained at a rate of 0.5C indicative of poor cyclic stability. The long-term cycling performance of the HPCMs/S and sublimed S cathodes is presented in Fig. 5e which indicates that the HPCMs/S cathode has better electrochemical stability than the sublimed S cathode.

Fig. 6a shows the long term cycling performance of the HPCMs/S cathode and sublimed S cathode at a current density of 1C. The HPCMs/S cathode shows a specific capacity of 728 mAh g^{-1} at a rate of 1C and the capacity could be maintained at 707 mAh g^{-1} after 200 cycles with the capacity decay of 0.014% per cycle. However, the sublimed S cathode delivers a lower capacity of 330 mAh g^{-1} after 200 cycles with only 46% capacity retention. These results demonstrate the good cycling stability of the HPCMs/S cathode. Fig. 6b displays the rate capability of the HPCMs/S cathode and sublimed S cathode, revealing that the HPCMs/S cathode delivers higher capacities at the measured current density compared to the sublimed S cathode. The HPCMs/S cathode shows a discharge capacity of 985 mAh g^{-1} at a rate of 0.1C as well as discharge capacity of 846 mAh g^{-1} at 0.2C. When the current density is increased from 0.2C to 4C, 527 mAh g^{-1} of the capacity is maintained corresponding to 62.3% of capacity retention. Moreover, when the current density is reverted back to 0.2C, the capacity of 839 mAh g^{-1} is retained, implying good reversibility. Compared with the HPCMs/S cathode, the sublimed S cathode demonstrates the lower capacities at the measured current densities, further corroborating better rate capability of HPCMs/S cathode. Fig. 6c–e depict the EIS profiles of the sublimed S and HPCMs/S cathodes before and after cycling 100 times at a rate of 0.5C between 100 kHz and 0.01 Hz together with the corresponding equivalent circuit model. The Nyquist plots consist of two depressed semicircles in the high and middle frequency regions

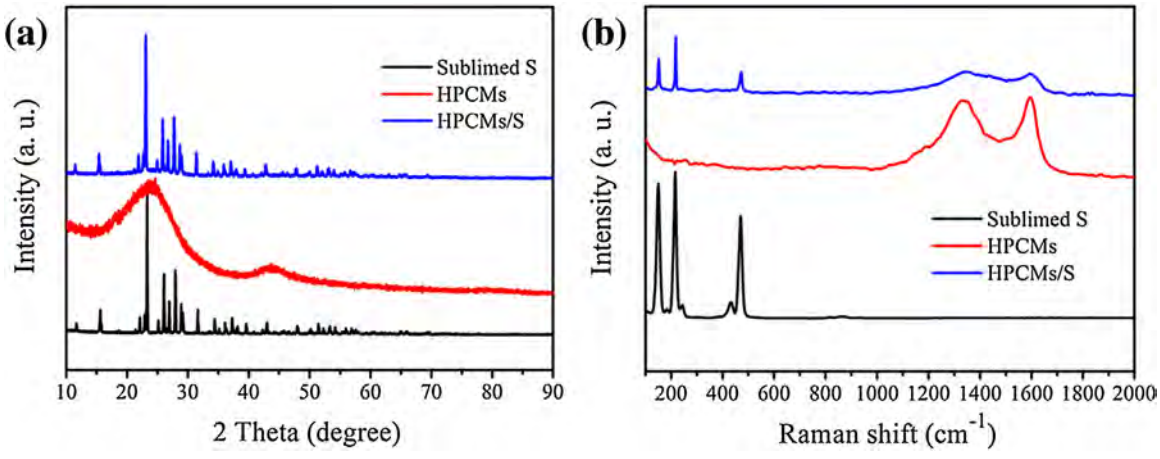

Fig. 4. (a) XRD patterns and (b) Raman scattering spectra of sublimed S, HPCMs, and HPCMs/S composites.

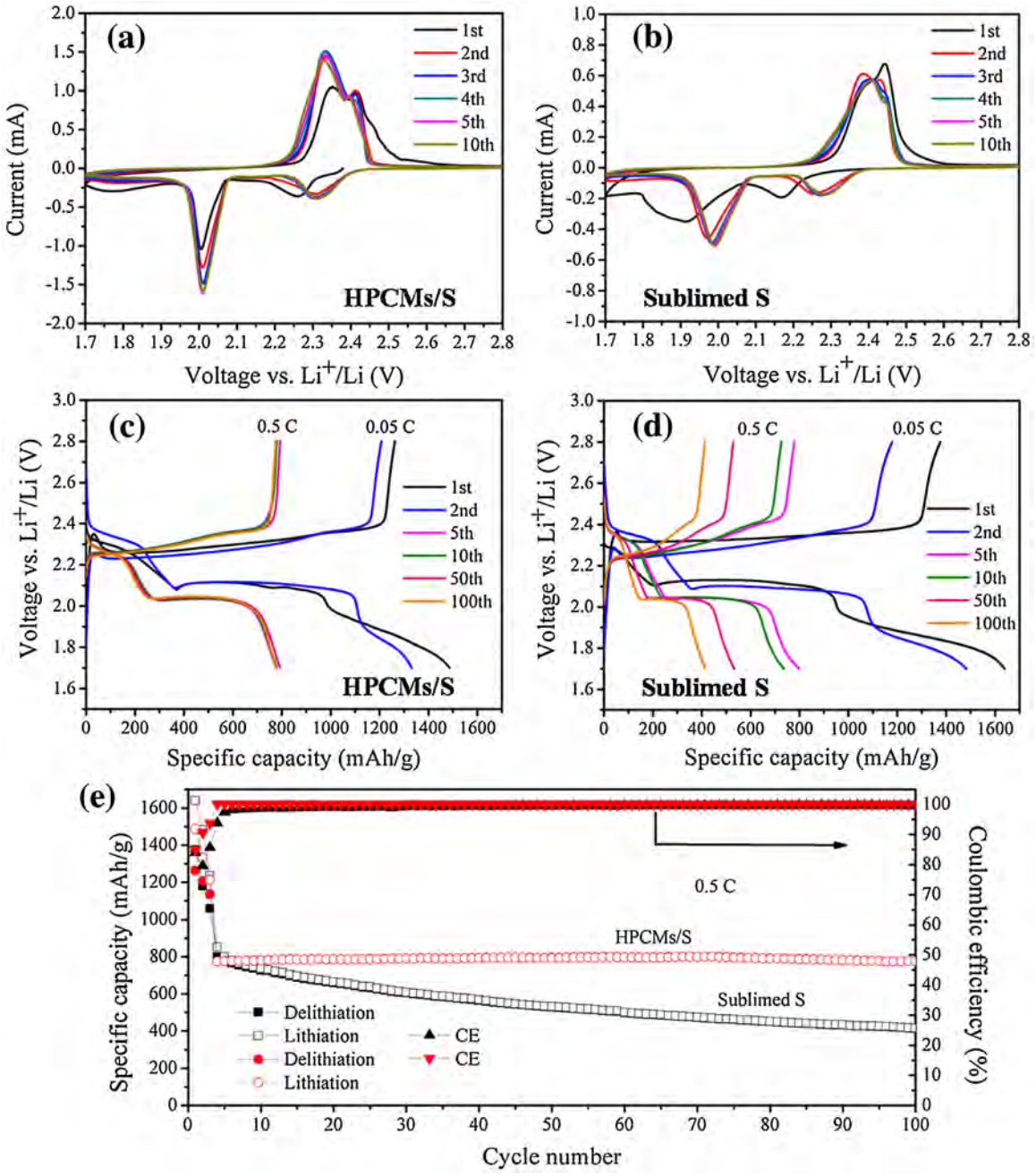

Fig. 5. CV profiles of the HPCMs/S cathode (a) and sublimed S cathode (b) at a scanning rate of 0.1 mV s^{-1}; GCD curves of the HPCMs/S cathode (c) and sublimed S cathode (d); (e) Long-term cycling performance of the two cathodes at a 0.5C rate (1 C = 1675 mA g^{-1}). The first 3 cycles were tested at a small activated rate of 0.05C.

after 100 cycles but only one semicircle before cycling. The first semicircle at high frequencies is attributed to the resistance of the solid electrolyte interface formed on the electrode surface (R_s) [41–47]. The HPCMs/S electrode has an R_s of 8.6 Ω that is smaller than that of the sublimed S electrode (170.4 Ω) after 100 cycles. The second semicircle in the medium frequency region is ascribed to the charge transfer resistance (R_{ct}) [48,49]. The R_{ct} values of the HCMs/S electrode are 42.6 and 28.4 Ω before and after 100 cycles, respectively, which are less than those of the sublimed S cathode (518.0 and 275.2 Ω before and after 100 cycles), implying easy charge transportation in the electrochemical reactions of the HCMs/S electrode as a result of the good conductivity.

We compare the electrochemical performance of the HPCMs/S cathode (the current work) with other related state-of-the-art S cathodes based on carbon host materials, which is depicted in Table 1. Although the HPCMs have a BET surface area of 284 $m^2 g^{-1}$ and pore volume of 0.6 $cm^3 g^{-1}$, the HPCMs/S composite shows significant improvement of the electrochemical performance in terms of the capacity, cycling stability and rate capability. The overall mass loading of S in the HPCMs/S composite is 70.26 wt.% according to the TG result shown in Fig. 3. The density of sublimed S is 2.07 g cm^{-3} and pore volume of HPCMs is 0.6 $cm^3 g^{-1}$, thus, 55.4 wt.% S was impregnated into the pores of HPCMs and about 14.8 wt. % of S was coated on the surface of HPCMs. However, the HPCMs derived from the bamboo leaves exhibit strong absorption ability toward polysulfide due to the presence of N-containing function groups and hierarchical inter-connected carbon network. XPS results of the HPCMs are shown in Fig. S4. The peaks at 284.6, 285.5, and 289.0 eV are attributed to C—C/C=C, C—N/C-O, O—C=O, and the peaks at 398.4, 399.6 and 400.9 eV correspond

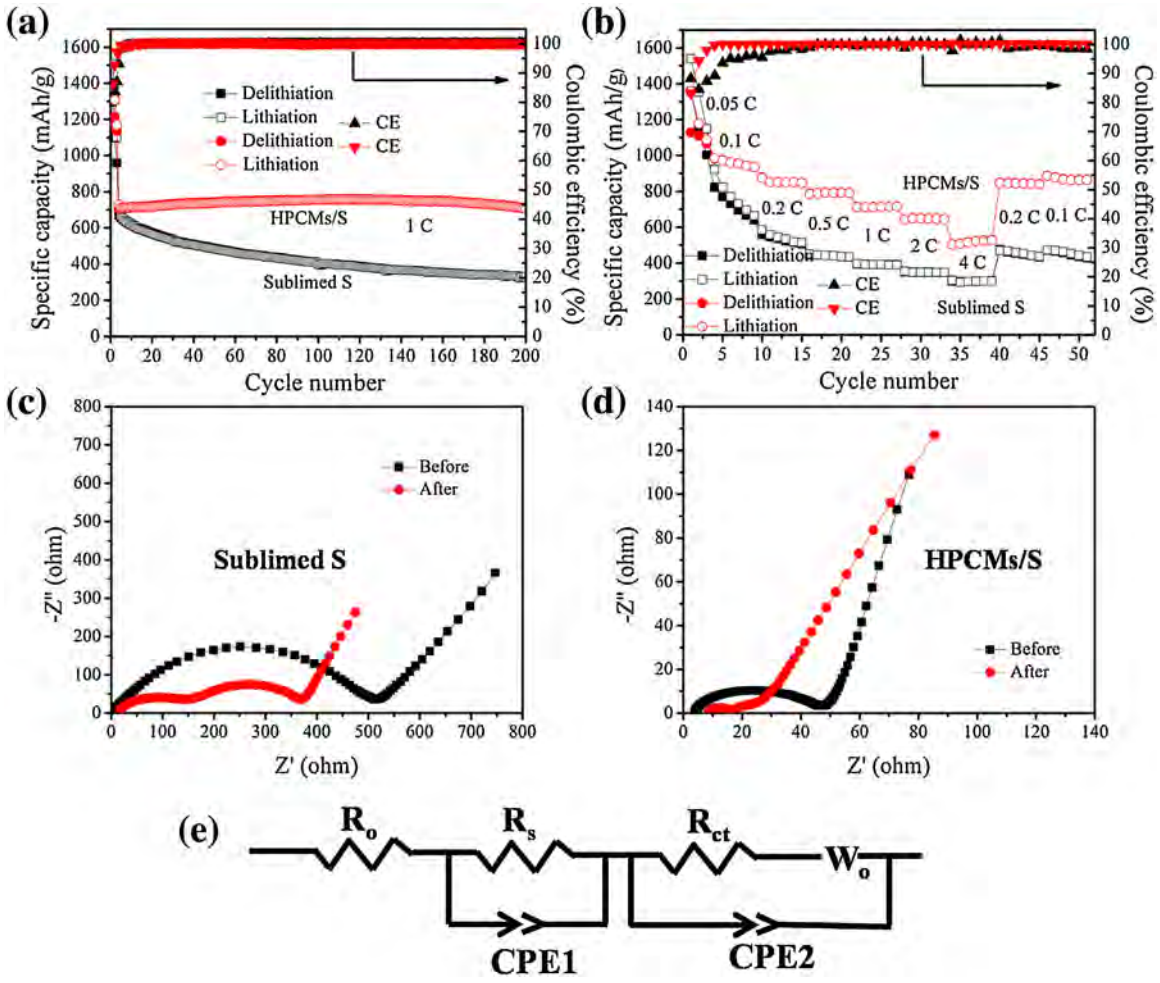

Fig. 6. Long-term cycling performance at a 1C rate (a) and Rate capability (b) of the HPCMs/S cathode and sublimed S cathode; EIS profiles of (c) sublimed S and (d) HPCMs/S cathodes before and after 100 cycles at 0.5C between 100 kHz and 0.01 Hz; (e) Corresponding equivalent circuit model.

Table 1
Comparisons of electrochemical performance of HPCMs/S composites with previously-reported C/S composites for Li-S batteries.

Materials	Additional Template (Yes or No)	KOH Activation (Yes or No)	Carbon Source	Process	Cycling Stability	Capacity Retention	Rate Capability
CSEM-Li_2S_6 [50]	No	Yes	Eggshell membrane	Simple	1000 mAh g^{-1} after 100 cycles at 0.1 C	75%	–
WSC/S [51]	No	Yes	Wheat straw	Complex	445 mAh g^{-1} after 200 cycles at 1 C	78%	432 mAh g^{-1} at 2 C
a-LSs/S [52]	No	Yes	Litchi shells	Complex	665 mAh g^{-1} after 100 cycles at 0.8 A g^{-1}	73%	580 mAh g^{-1} at 3.2 A g-1
S/ACF [53]	No	Yes	Pomelo peel	Complex	750 mAh g^{-1} after 100 cycles at 0.2 C	60%	700 mAh g^{-1} at 2 C
SFC/S [54]	No	Yes	Cocoons	Complex	567 mAh g^{-1} after 200 cycles at 1 C	91%	477 mAh g^{-1} at 2 C
S/PC [55]	Yes	No	Sucrose	Simple	504 mAh g^{-1} after 200 cycles at 0.5 C	69%	516 mAh g^{-1} at 2 C
S/PMC [56]	Yes	No	Aniline	Complex	486 mAh g^{-1} after 200 cycles at 1 C	64%	425 mAh g^{-1} at 2 C
PDA-NHC-S [57]	Yes	No	Dopamine	Complex	700 mAh g^{-1} after 200 cycles at 0.6 C	94%	–
S/N-HPCB [58]	Yes	No	RB	Complex	702 mAh g^{-1} after 200 cycles at 1 C	78%	673 mAh g^{-1} at 2 C
KFCNTs/S [59]	No	No	Kapok fibers	Simple	524 mAh g^{-1} after 90 cycles at 0.4 A g^{-1}	95%	445 mAh g^{-1} at 1 A g^{-1}
HPCMs/S (This work)	No	No	Bamboo leaves	Simple	707 mAh g^{-1} after 200 cycles at 1 C	97%	649 mAh g^{-1} at 2 C

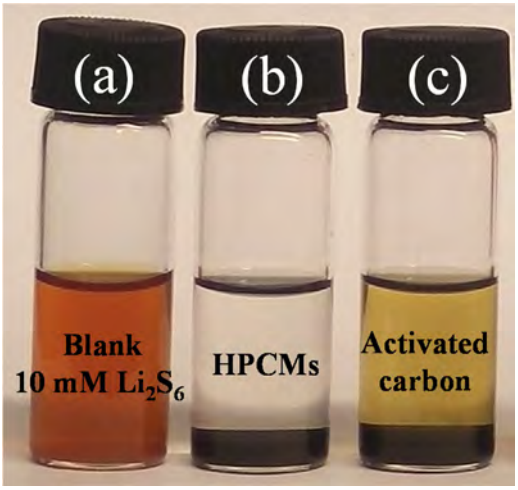

Fig. 7. Optical photographs of polysulfide adsorption by adding different carbon materials. (a) Pristine 10 mM Li_2S_6 solution, blank; (b) 10 mM Li_2S_6 solution after adding HPCMs and (c) 10 mM Li_2S_6 solution after being adsorbed by activated carbon with a surface area of 1800 $m^2 g^{-1}$.

to pyridinic, pyrrolic, and quaternary N, respectively [58,60,61]. The N- and O- functional groups in HPCMs boast polar interaction and strong absorption between HPCMs and polysulfide, refraining the polysulfide loss and shuttle and resulting in excellent electrochemical properties [62,63]. We compared the adsorption ability of the our HPCMs and active carbon (surface area of 1800 $m^2 g^{-1}$ and pore volume of 0.9 $cm^3 g^{-1}$, purchased from Shanghai Sino Tech Investment Management Co., Ltd., China) toward polysulfide and the results are shown in Fig. 7. The orange Li_2S_6 solution (10 mM) is prepared in a mixture solution of DOL/DME (1/1, V/V) by using sublimed sulfur powders and lithium sulfide (Li_2S) under stirring for 24 h. Then 40 mg of HPCMs or activated carbon is added into 3 mL of Li_2S_6 solution. After the HPCMs powders were added, the color of the polysulfide solution changes from orange to colorless, but the color of polysulfide solution changes white yellow from orange after adding active carbon with area of 1800 $m^2 g^{-1}$ and pore volume of 0.9 $cm^3 g^{-1}$. These results confirm that the HPCMs have stronger adsorption ability toward polysulfide than active carbon although it has much larger surface area and pore volume. The hierarchical interconnected carbon network and strong absorption ability of HPCMs toward polysulfide boast the excellent electrochemical properties of HPCMs/S for Li-S batteries. On the other hand, compared with previously-reported porous carbon materials that are generally need KOH chemical acitivation or use foreign templates to produce meso-/microporos carbon materials, our method uses the biogenetic SiO_2 self-templates in the bamboo leaves to produce HPCMs and the preparation procedure is simple, which is potential applications to advanced Li-S batteries.

4. Conclusion

Hierarchically porous carbon materials are prepared in a large scale from waste biomass of bamboo leaves by carbonization and HF etching to remove the biogenetic mesoporous SiO_2 nanoparicles. The HPCMs/S composite with 70.26 wt.% sulfur exhibits a large initial specific capacity of 1487 mAh g^{-1} at 0.05C and the specific capacity is maintained at 707 mAh g^{-1} at a 1C for over 200 cycles. When the current density is increased 20 times from 0.2C to 4C, 62.3% of the capacity is retained. The low-cost and high-efficiency hierarchical porous carbon materials derived from bamboo leaves have large potential in Li−S batteries.

Acknowledgements

This work was financially supported by National Natural Science Foundation of China (Nos. 52572100 and 51504171), Natural Science Foundation of Hubei Province (2015CFA116), Fundamental Research Funds for the Central Universities (HUST: 2015QN071), HUST Key Interdisciplinary Team Project (2016JCTD101), Outstanding Young and Middle-aged Scientific Innovation Team of Colleges and Universities of Hubei Province (T201402), and City University of Hong Kong Applied Research Grant (ARG) No. 9667122. The authors also acknowledge the Nanodevices and Characterization Center of WNLO-HUST and Analytical and Testing Center of HUST.

Appendix A. Supplementary data

Supplementary data associated with this article can be found, in the online version, at http://dx.doi.org/10.1016/j.electacta.2017.01.166.

References

[1] F. Wu, H. Kim, A. Magasinski, J.T. Lee, H.T. Lin, G. Yushin, Adv. Energy Mater. 4 (2014) 100196–1400202.
[2] R. Xu, J. Lu, K. Amine, Adv. Energy Mater. 5 (2015) 1500408–1500429.
[3] C. Nan, Z. Lin, H. Liao, M.-K. Song, Y. Li, E.J. Cairns, J. Am. Chem. Soc. 136 (2014) 4659–4663.
[4] G. Xu, B. Ding, J. Pan, P. Nie, L. Shen, X. Zhang, J. Mater. Chem. A 2 (2014) 12662–12676.
[5] Y. Zhao, W. Wu, J. Li, Z. Xu, L. Guan, Adv. Mater. 26 (2014) 5113–5118.
[6] M. Yu, W. Yuan, C. Li, J.-D. Hong, G. Shi, J. Mater. Chem. A 2 (2014) 7360–7366.
[7] J. Wang, L. Yin, H. Jia, H. Yu, Y. He, J. Yang, C.W. Monroe, ChemSusChem 7 (2014) 563–569.
[8] K. Liao, P. Mao, N. Li, M. Han, J. Yi, P. He, Y. Sun, H. Zhou, J. Mater. Chem. A 4 (2016) 5406–5409.
[9] M.Q. Zhao, M. Sedran, Z. Ling, M.R. Lukatskaya, O. Mashtalir, M. Ghidiu, B. Dyatkin, D.J. Tallman, T. Djenizian, M.W. Barsoum, Y. Gogotsi, Angew. Chem. Int. Ed. 54 (2015) 4810–4814.
[10] Z. Li, C. Li, X. Ge, J. Ma, Z. Zhang, Q. Li, C. Wang, L. Yin, Nano Energy 23 (2016) 15–26.
[11] R. Fang, S. Zhao, S. Pei, X. Qian, P.-X. Hou, H.-M. Cheng, C. Liu, F. Li, ACS Nano 10 (2016) 8676–8682.
[12] M.K. Song, Y. Zhang, E.J. Cairns, Nano Lett. 13 (2013) 5891–5899.
[13] S. Yuan, J.L. Bao, L. Wang, Y. Xia, D.G. Truhlar, Y. Wang, Adv. Energy Mater. 6 (2016) 1501733–1501741.
[14] G. Zhou, L.C. Yin, D.W. Wang, L. Li, S. Pei, I.R. Gentle, F. Li, H.M. Cheng, ACS Nano 7 (2013) 5367–5375.
[15] S. Xin, L. Gu, N.H. Zhao, Y.X. Yin, L.J. Zhou, Y.G. Guo, L.J. Wan, J. Am. Chem. Soc. 134 (2012) 18510–18513.
[16] Z. Yuan, H.J. Peng, J.Q. Huang, X.Y. Liu, D.W. Wang, X.B. Cheng, Q. Zhang, Adv. Funct. Mater. 24 (2014) 6105–6112.
[17] L. Miao, W. Wang, K. Yuan, Y. Yang, A. Wang, Chem. Commun. 50 (2014) 13231–13234.
[18] R. Fang, S. Zhao, P. Hou, M. Cheng, S. Wang, H.M. Cheng, C. Liu, F. Li, Adv. Mater. 28 (2016) 3374–3382.
[19] W. Chen, Z. Zhang, Q. Li, Y. Lai, J. Li, ChemElectroChem 2 (2015) 246–252.
[20] S. Rehman, X.X. Gu, K. Khan, N. Mahmood, W. Yang, X.X. Huang, S.J. Guo, Y.L. Hou, Adv. Energy Mater. 6 (2016) 1502518–15025525.
[21] G. Li, J. Sun, W. Hou, S. Jiang, Y. Huang, J. Geng, Nat. Commun. 7 (2016) 10601–10610.
[22] X. Ji, K.T. Lee, L.F. Nazar, Nat. Mater. 8 (2009) 500–506.
[23] Z. Li, Y. Jiang, L. Yuan, Z. Yi, C. Wu, Y. Liu, P. Strasser, Y.H. Huang, ACS Nano 8 (2014) 9295–9303.
[24] S. De, A.M. Balu, J.C. van der Waal, R. Luque, ChemCatChem 7 (2015) 1608–1629.
[25] H. Ye, Y.X. Yin, S. Xin, Y.G. Guo, J. Mater. Chem. A 1 (2013) 6602–6608.
[26] H. Feng, H. Hu, H. Dong, Y. Xiao, Y. Cai, B. Lei, Y. Liu, M. Zheng, J. Power Sources 302 (2016) 164–173.
[27] H. Wang, Z. Xu, A. Kohandehghan, Z. Li, K. Cui, X. Tan, T.J. Stephenson, C.K. King'ondu, C.M.B. Holt, B.C. Olsen, J.K. Tak, D. Harfield, A.O. Anyia, D. Mitlin, ACS Nano 7 (2013) 5131–5141.
[28] X.Y. Zheng, W. Lv, Y. Tao, J.J. Shao, C. Zhang, D.H. Liu, J.Y. Luo, D.W. Wang, Q.H. Yang, Chem. Mater. 26 (2014) 6896–6903.
[29] M. Wahid, D. Puthusseri, D. Phase, S. Ogale, Energy Fuels 28 (2014) 4233–4240.
[30] Y. Qu, Z. Zhang, X. Zhang, G. Ren, X. Wang, Y. Lai, Y. Liu, J. Li, Electrochim. Acta 137 (2014) 439–446.
[31] M. Umemura, C. Takenaka, Ecol. Res. 29 (2014) 501–510.
[32] L. Wang, B. Gao, C.J. Peng, X. Peng, J.J. Fu, P.K. Chu, K.F. Huo, Nanoscale 7 (2015) 13840–13847.

[33] K.W. Kow, R. Yusoff, A.R.A. Aziz, E.C. Abdullah, J. Non-Cryst. Solids 386 (2014) 76–84.
[34] D.S. Jung, M.-H. Ryou, Y.J. Sung, S.B. Park, J.W. Choi, PNAS 110 (2013) 12229–12234.
[35] M. Biswai, A. Banerjee, M. Deo, S. Ogale, Energy Environ. Sci. 6 (2013) 1249–1259.
[36] S.S. Zhang, J. Electrochem. Soc. 159 (2012) A920–A923.
[37] A. Rosenman, R. Elazari, G. Salitra, E. Markevich, D. Aurbach, A. Garsuch, J. Electrochem. Soc. 162 (2015) A470–A473.
[38] X. Gu, Y. Wang, C. Lai, J. Qiu, S. Li, Y. Hou, W. Martens, N. Mahmood, S. Zhang, Nano Res. 8 (2015) 129–139.
[39] B. Zhang, X. Qin, G.R. Li, X.P. Gao, Energy Environ. Sci. 3 (2010) 1531–1537.
[40] S.S. Zhang, Front. Energy Res. 1 (2013) 1–9.
[41] J. Zhou, N. Lin, W.L. Cai, C. Guo, K.L. Zhang, J.B. Zhou, Y.C. Zhu, Q.T. Qian, Electrochim. Acta 218 (2016) 243–251.
[42] W.L. Zhai, W.L. Tu, Y. Liu, H.Y. Gao, J.G. Yu, Y.N. Zhao, G.D. Li, Electrochim. Acta 219 (2016) 143–151.
[43] J. Xie, J. Yang, X.Y. Zhou, Y.L. Zou, J.J. Tang, S.C. Wang, F. Chen, J. Power Sources 253 (2014) 55–63.
[44] H. Li, L.P. Sun, G.C. Wang, ACS Appl. Mater. Interfaces 8 (2016) 6061–6071.
[45] S.M. Zhang, Q. Zhang, J.Q. Huang, X.F. Liu, W.C. Zhu, M.Q. Zhao, W.Z. Qian, F. Wei, Part. Part. Syst. Charact. 30 (2013) 158–165.
[46] J. Yan, X. Liu, M. Yao, X. Wang, T.K. Wafle, B. Li, Chem. Mater. 27 (2015) 5080–5087.
[47] Z. Deng, Z. Zhang, Y. Lai, J. Liu, J. Li, Y. Liu, J. Electrochem. Soc. 160 (2013) A553–A558.
[48] B. Zhang, M. Xiao, S. Wang, D. Han, S. Song, G. Chen, Y. Meng, ACS Appl. Mater. Interfaces 6 (2014) 13174–13182.
[49] J. Li, F. Qin, L. Zhang, K. Zhang, Q. Li, Y. Lai, Z. Zhang, J. Fang, J. Mater. Chem. A 2 (2014) 13916–13922.
[50] S.H. Chung, A. Manthiram, Adv. Mater. 26 (2014) 1360–1365.
[51] Y.M. Cheng, S.M. Ji, X.J. Xu, J. Liu, RSC Adv. 5 (2015) 10089–100096.
[52] S.T. Zhang, M.B. Zheng, Z.X. Lin, N.W. Li, Y.J. Liu, B. Zhao, H. Pang, J.M. Cao, P. He, Y. Shi, J. Mater. Chem. A 2 (2014) 15889–15896.
[53] J. Zhang, J.Y. Xiang, Z.M. Dong, Y. Liu, Y.S. Wu, C.M. Xu, G.H. Du, Electrochim. Acta 116 (2014) 146–151.
[54] J.W. Zhang, Y.R. Cai, Q.W. Zhong, D.Z. Lai, J.M. Yao, Nanoscale 7 (2015) 17791–17797.
[55] G.L. Xu, Y.F. Xu, J.C. Fang, X.X. Peng, F. Fu, L. Huang, J.T. Li, S.G. Sun, ACS Appl. Mater. Interfaces 5 (2013) 10782–10793.
[56] X.H. Zhao, Y. Liu, J. Manuel, G.S. Chauhan, H.J. Ahn, K.W. Kim, K.K. Cho, J.H. Ahn, ChemSusChem 8 (2015) 3234–3241.
[57] W.D. Zhou, X.C. Xiao, M. Cai, L. Yang, Nano Lett. 14 (2014) 5250–5256.
[58] F. Pei, T.H. An, J. Zang, X.J. Zhao, X.L. Fang, M.S. Zheng, Q.F. Dong, N.F. Zheng, Adv. Energy Mater. 6 (2016) 1502539–1502546.
[59] X.Y. Tao, J.T. Zhang, Y. Xia, H. Huang, J. Du, H. Xiao, W.K. Zhang, Y.P. Gan, J. Mater. Chem. A 2 (2014) 2290–2296.
[60] Q.F. Cai, Y.Y. Li, L. Wang, Q.W. Li, J. Xu, B. Gao, X.M. Zhang, K.F. Huo, P.K. Chu, Nano Energy 32 (2017) 1–9.
[61] Z.H. Sheng, L. Shao, J.J. Chen, W.J. Bao, F.B. Wang, X.H. Xia, ACS Nano 5 (2011) 4350–4358.
[62] T.Z. Hou, X. Chen, H.J. Peng, J.Q. Huang, B.Q. Li, Q. Zhang, B. Li, Small 12 (2016) 3283–3291.
[63] C. Luo, Y.J. Zhu, O. Borodin, T. Gao, X.L. Fan, Y.H. Xu, K. Xu, C.S. Wang, Adv. Funct. Mater. 26 (2016) 745–752.

Supporting Information

Hierarchical Porous Carbon Materials Derived from Self-Template Bamboo Leaves for Lithium–Sulfur Batteries

Yuanyuan Li [a], Lei Wang [a], Biao Gao [b], Xingxing Li [b], Qifa Cai [a], Qingwei Li [a,c], Xiang Peng [c], Kaifu Huo [a,*], Paul K Chu [c,*]

[a] Wuhan National Laboratory for Optoelectronics and School of Optical and Electronic information, Huazhong University of Science and Technology, Wuhan 430074, People's Republic of China

[b] The State Key Lab for Refractory and Metallurgy, Wuhan University of Science and Technology, Wuhan 430081, People's Republic of China

[c] Department of Physics and Materials Science, City University of Hong Kong, Tat Chee Avenue, Kowloon, Hong Kong, China

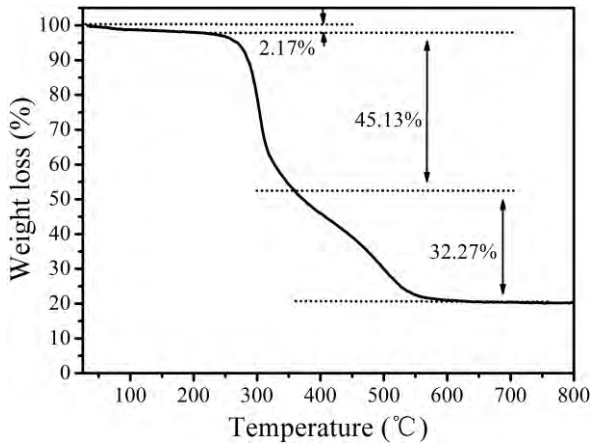

Fig. S1. Thermogravimetric analysis (TGA) curve of HCl-etched bamboo leaves from room temperature to 800 ºC with the heating rate of 5 ºC/min under Ar/O_2 atmosphere.

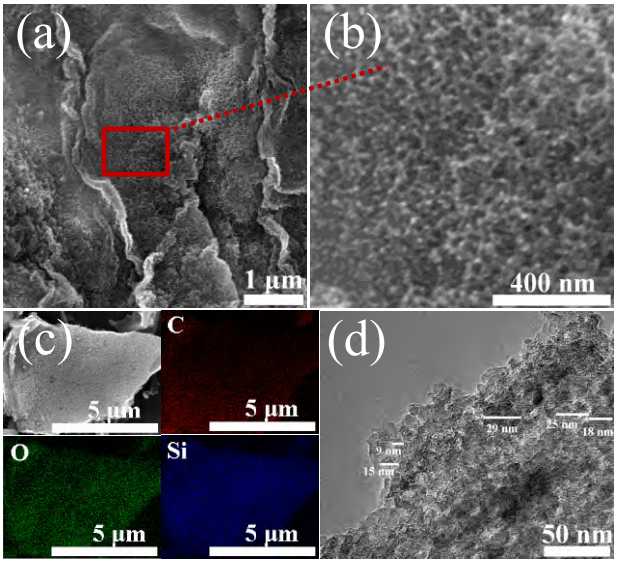

Fig. S2. (a and b) low and magnification FE-SEM images of carbonized HCl-etched bamboo leaves; (c) EDS mappings; (d) TEM image.

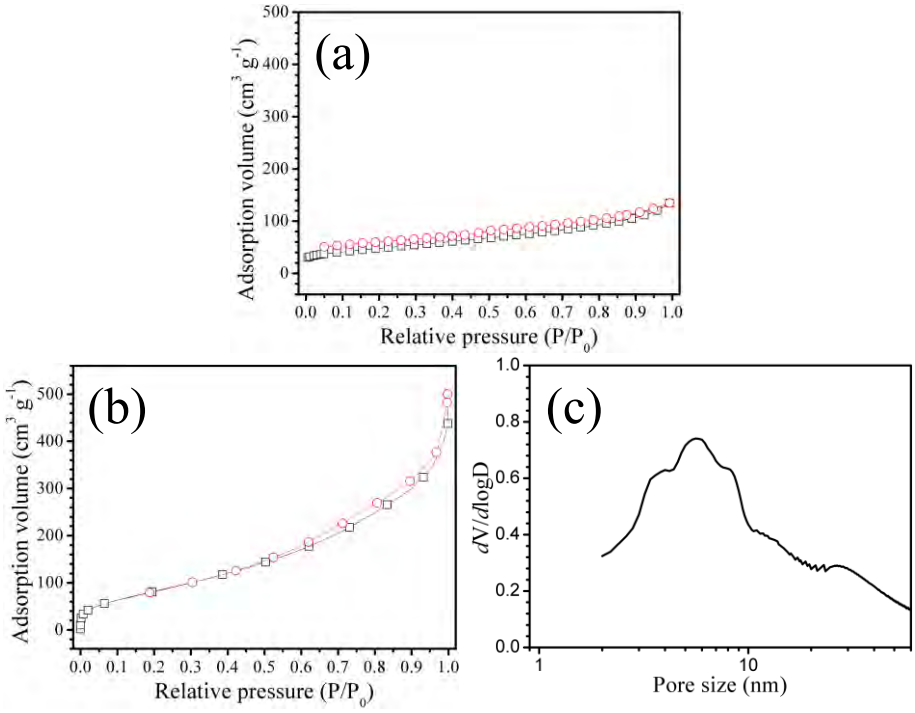

Fig. S3. Nitrogen adsorption-desorption isothermal curves of carbonized HCl-etched bamboo leaves (a) and SiO_2 nanoparticles (after the removal of the carbon in bamboo leaves in air under 700 ºC for 2 h) (b) and corresponding pore size distribution plots (c) of SiO_2 nanoparticles.

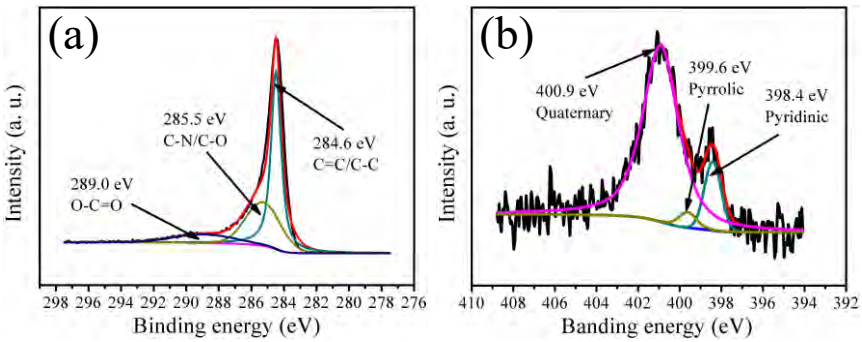

Fig. S4. X-ray photoelectron spectroscopy (XPS) of the HCPMs. Fine XPS of (a) C1s and (b) N1s.